Periodicity in the historical light curve of the LBV star η Carinae

Ts. B. Georgiev[1], A. Valcheva[2], P. Nedialkov[2],
S. Stefanov[2,3] and M. Moyseev[3]
[1]New Bulgarian University, 21 Montevideo Blvd., 1618 Sofia, Bulgaria
[2]Department of Astronomy, Faculty of Physics, Sofia University "St. Kliment Ohridski",
5 James Bourchier Blvd., 1164 Sofia, Bulgaria
[3]Institute of Astronomy and National Astronomical Observatory,
Bulgarian Academy of Sciences, 72 Tsarigradsko Chaussee Blvd., 1784 Sofia, Bulgaria
japet@phys.uni-sofia.bg
(Submitted on 7 May 2024; Accepted on 10 February 2025)

Abstract. We search for periods in a compiled two centuries historical light curve (1823–2023) of η Carinae in BV band, applying four periodogram methods. The Structure Eminence Function (SEF) marks the positions of the significant repetitive structures (humps in the function), responsible for quasi-periods. Its "derivative" - the Periodograph Function (PGF) makes the humps manifest more clearly, since it is a normalized SEF with subtracted background, which yields a spectrum of the quasi-periods and periods, analogues to the power spectrum of the other methods. The periodogram methods CLEAN and Lomb-Scargle are also used in a comparative framework.

Our analysis yields two prominent periods in the selected three data sets – "earlier" included V-band photometry from 1866 to 1926 and "recent" which includes B and V-band photometry from 1963–2023. One of the periods that can be linked to the well established orbital period of the system is conspicuous in all data sets and has value of $P_1 = 5.6 \pm 0.1$ yr in the "earlier" data and $P_1 = 5.7 \pm 0.1$ yr in the "recent" data. Since the difference of 0.1 yr between these periods does not depend on the methods we use, it may hint at a period increase over one century.

A less prominent period of $P_2 = 4.9 \pm 0.1$ yr is also detected in the three data sets. This period is well pronounced in all V-band data and less prominent in "recent" B-band data. CLEAN and Lomb-Scargle methods applied on the same three data sets yield results that coincide with the SEF and PGF results. This shorter period may be explained by a geometric effect manifesting in the light curve of η Car.

Key words: LBV stars; light curves: quasi-periods; LBV stars; η Car.

Introduction

Located at a distance of 2.35 kpc (Smith 2006, Shull et al. 2021), η Carinae is a nearby LBV star considered to be a single-lined spectroscopic binary system with a highly eccentric orbit (e$\sim$0.9) and with a total luminosity $\sim 5 \times 10^6 L_\odot$. In 2011, it had V=4.3 mag and currently η Car is a 4th mag star. However, during its "Great Eruption" between 1837 and 1843, it reached a brightness of about –1 mag. After 1856, its brightness dropped well below naked-eye visibility, with the exception of a smaller eruption around 1892, during which it reached 6th mag. Since 1941, η Car's brightness exhibited a gradual increase (O'Connell 1956).

Van Genderen et al. (2006) claim to have found the precisest period of 5.535 $\pm$ 0.001 yr in their comprehensive study of the peaks and dips during the so-called "events" of extreme UBV and/or NIR brightness of η Car. That period is obtained by matching the ascending branches of the UBV light curve peaks during the events in 2003.5 and 1981.3. The authors also verified oscillations between 200 d and 400 d, probably related to stellar pulsations of the primary. Damineli et al. (1997) were the first to produce time series for the equivalent

width of the following lines in η Car's spectrum: He I 6678 narrow component, Si II 6347, He I 10830 and Fe II 6455 P Cygni line, as well for the radial velocity of Fe II 6455 P Cygni and He I 6678 broad component. They have combined all available original and literature data spanning over 60 yr and determined a well-defined period of 5.538 ± 0.003 yr. This period is believed to be the orbital period in the binary system of η Car. The first direct evidences for the possible Wolf–Rayet nature of the hot unresolved companion were obtained by Strawn et al. (2023) who detected He II 4686 emission line motion in direction opposite to the the primary star away from the phases of closest approach.

Recently, modeling of colliding winds with a certain opening angle and apex location of a hyperboloid (Grant et al. 2023) led to the conclusion that the binary is oriented with the companion on the observer's side of the system during apastron. Morse & Smith (2024) found a relatively fast, low-density polar wind that preceded by several decades the fast and dense wind of the Homunculus. They favor with caution the Great Eruption model of a merger in a hierarchical triple system (Smith et al. 2018). According to that model, the bipolar shape of the Homunculus formed when the merger debris collided with a dense torus ejected earlier during the inspiral phase before the merger. The alternative hypothesis (Hirai et al. 2021) states that the bipolar shape of Homunculus is due to a prolate super-Eddington wind from the rapidly rotating post-merger star.

The paper is organized as follows: after a brief introduction on the topic, Section 1 describes the sources of photometric data used in the construction of the historical light curve (1866–2023) of η Car. Section 2 provides a summary of the Structure eminence function (SEF) method and its derivative - Periodograph Function (PGF). Some basic information on CLEAN and Lomb-Scargle periodogram methods is also included. In Section 3, we present the results from SEF and PGF methods, as well as the results from the CLEAN and Lomb-Scargle application. Some discussion of the detected periods is included in Section 4. The paper ends with some concluding remarks.

1 The historical light curve of η Car and the selection of time series

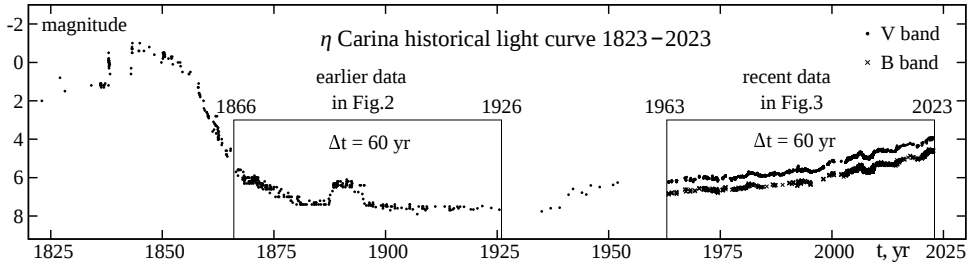

Fig. 1. Two centuries-long historical light curve of η Car in B and V bands

We compile two centuries-long historical light curve (LC thereafter) of η Car since 1823 until 2023 (Fig.1) using BV photometry published in Fernández-Lajús et al. (2009) and photometry from the AAVSO light curve generator[1] in the same bands. Both sources of data include photometry published by different authors and different AAVSO observing groups - Auckland Photometric Observers Group, New Zealand (APOG), Arie Verveer, Australia (VARA), Libert Monard, South Africa (MLF), and Giorgio di Scala, Australia (DSI).

We selected three datasets within two 60-yr long intervals, namely, 1866–1926 and 1963–2023 for further analysis. These are the parts with the best coverage in the historical LC compiled by us. We call them "earlier" and "recent" data sets. The "earlier" data set includes two sources of photometry (Hoffleit 1933, Frew 2004) and contains photometry solely in V band taken directly from the LC of η Car as given in Fernández-Lajús et al. (2009) and contains 301 photometric points. The "recent" data contain photometry both in B and V band. B-band data set includes eight sources of photometry and 2262 data points in total, while the V-band set includes 10 sources and 2375 data points. We specified the sources of photometry, time span and the number of points for the "recent" data sets in Table 1.

Table 1. Sources of "recent" photometry data: eight in B band and 10 in V band.

Source	Time span	Number of measurements
Feinstein (1967)	1963.41 – 1967.45	18
Feinstein & Marraco (1974)	1968.23 – 1973.24	17
van Genderen et al. (2006)/Auckland	1971.23 – 2005.60	219
van Genderen et al. (2006)/Blenheim	1990.49 – 2006.85	145
Fernández-Lajús et al. (2009)	2003.05 – 2008.67	586
VARA (AAVSO)	2008.24 – 2009.43	603
MLF (AAVSO)	2020.37 – 2022.75	261
DSI (AAVSO)	2005.27 – 2022.45	413
		Total B: 2262
Feinstein (1967)	1963.41 – 1967.45	18
Feinstein & Marraco (1974)	1968.23 – 1973.24	21
Sterken et al. (1996)	1977.21 – 1991.14	131
Sterken et al. (1999)	1992.10 – 1999.25	205
van Genderen et al. (2006)	1971.22 – 2000.19	259
Fernández-Lajús et al. (2009)	2003.05 – 2008.67	662
APOG (AAVSO)	2002.07 – 2002.13	3
VARA (AAVSO)	2008.24 – 2009.43	568
MLF (AAVSO)	2020.37 – 2022.75	91
DSI (AAVSO)	2005.27 – 2022.45	417
		Total V: 2375

Homogenization of the LCs was implemented applying small corrections (0.042–0.113 mag) to account for systematic differences (all measured with uncertainty less than 0.015 mag) between Fernández-Lajús et al. (2009) magnitudes (B_{FL} and V_{FL}) and the magnitudes of AAVSO groups MLV and DSI indexed with the corresponding subscripts, as follows:

[1] https://www.aavso.org/LCGv2/

B band:
$B_{FL} = B_{DSI}$ – 0.070 (for t $\leq$ 2006.7 yr)
$B_{FL} = B_{DSI}$ – 0.042 (for t $>$ 2006.7 yr)
$B_{FL} = B_{MLV}$ + 0.088

V band:
$V_{FL} = V_{DSI}$ – 0.113
$V_{FL} = V_{MLF}$ – 0.113

The shifts were derived within fragments of the LC where the AAVSO photometry overlaps with Fernández-Lajús et al. (2009) photometry which we used for the LC reference system of η Car and which is in perfect agreement with VARA and APOG data.

2 Methodology

2.1 Structure eminence and Periodograph functions

The search for periodicity in the three photometric data sets defined above is carried out by the use of the structure eminence function (SEF) method introduced by Georgiev (2023, hereafter G23) and its derivative – the Periodograph Function (PGF). Note that SEF was originally named "function of the structure length eminence (SLE)". SEF describes the relation between the modified amplitude E of the repetitive structure in the residual light curve (RLC) for a variable star and the time length t_L. Here, RLC is the difference between the resampled LC and its smoothed version. Structures with high internal amplitudes are called SEF humps and their time lengths correspond to the respective periods or quasi-periods (QPs). Note that we use the concept QPs in general, saving the term "period" for a QP which is recognized independently as a period by another method. When P is a prominent period, then its larger counterpart QPs $2P$, $3P$, etc. are periods too. The SEF method also reveals shorter counterpart QPs, mainly $P/2$ which are also easily identifiable.

The construction of the SEF begins with resampling the LC with a constant time step δt which resulting in an equidistant time series of stellar magnitudes $m(t)$ with N_0 data points, spanning a time interval $\delta t \times N_0$. Next, this resampled LC is averaged within a selected window size (WS) with a step δt, obtaining a smoothed LC $m_S(t)$ with a reduced length N. Finally, the RLC is obtained taking the difference between these two LCs:

$$\Delta m(t) = -[m(t) - m_S(t)]. \tag{1}$$

By construction its overall average is zero.

The method assumes that the RLC contains a repetitive structure spanning a hitherto unknown length of L data points, corresponding to a time interval $t_L = \delta t \times L$. To recover this structure, we probe the RLC for number of different structure lengths L dp within an interval (L_{min}, L_{max}); we construct for each of them the corresponding SEF $E(L)$ (or $E(t_L)$) as follows. First, for the given L, we select from the RLC the first L dp, creating an initial set with cell numbers $j = 1, L$. Then, we add to that set the next L dp from

the RLC, so the L+1^{st} RLC point is summed with the 1^{st} cell of the new set, the L+2^{nd} RLC point is summed with the 2^{nd} cell, etc. The maximum number additions, or the number of times the RLC folds over into the trial set is $k_L = N/L$ (truncated to an integer number). For at least $k_L = 2$ additions, the maximum probed data length is $L_{max} = N/2$ dp. For example, from the RLC shown in Fig. 2b which contains 541 dp, we have L_{min}=10 dp (1 yr) and L_{max}=541/2=270 dp (27 yr) for Fig. 2c.

So, for each L every j^{th} cell contains k_L times the Δm summand from RLC and we take a_j - the average value of Δm and its standard deviation d_j. Thus, we define the signal profile a_j and the noise profile d_j of a repetitive structure as functions of j (see Figs 2(g–j) and 3(d–j)).

Every such structure is characterized by a signal $A(L)$ and a noise $D(L)$ averaged over $j = 1, 2, ..., L$:

$$A(L) = \langle |a_j| \rangle_L, \qquad D(L) = \langle d_j \rangle_L. \tag{2}$$

Since the average signal $A(L)$ gathers the absolute values $|a_j|$, it is the average amplitude of the repetitive structure with length L, as well $D(L)$ is the average noise of this structure (G23).

In such way, every significant repetitive structure, with arbitrary profile, with length L dp produces a local maximum of $A(L)$ and a local minimum of $D(L)$. Therefore, the maximum of the ratio $A(L)/D(L)$ is a sensitive indicator of QP peaks, and dimensionless SEF is defined by the ratio:

$$E(L) = A(L)/D(L), \qquad E(t_L) = A(t_L)/D(t_L). \tag{3}$$

Initially, our method was designed for linearized LC, i.e. LC converted in fluxes. Then the RLC is represented in percentages towards the relevant smoothed LC (G23). However, if the studied LCs exhibit a significant rise in brightness, the histogram of the RLC, build in fluxes, has positive skewness. The histogram in magnitudes is closer to normal distribution and we consider that their mean value is close to zero. For this reason, we define RLCs in magnitude differences. Note that a magnitude difference, Δm (such as the SD of the RLC), may be converted into relative flux change $\delta F = \Delta F/F$ (and vise versa) by the formulae of Pogson:

$$\Delta m = 2.5 \times \log(\delta F + 1) \quad \text{or} \quad \delta F = \text{dex}(0.4 \times \Delta m) - 1. \tag{4}$$

In addition, the value of $\Delta m < 0.25$ mag, expressed in hundreds of a magnitude, corresponds approximately to the value of δF, expressed in fractions.

The SEF method was already tested and dozens QPs and several modes have been discovered in the LCs of the flickering symbiotic stars T CrB (Georgiev et al. 2021) and MWC 560 (Georgiev et al. 2022), and the nova-like cataclysmic star AQ Men (Georgiev, Zamanov & Stefanov 2023).

The search for periodic signals in the signal-to-noise regime is a straightforward way to analyze LCs. In the present study, we introduce a similar approach by reconfiguring SEF into a dimensionless $G(t_L)$ - Periodograph Function (PGF). The PGF is the difference between the SEF $E(t_L)$ and SEF

background $E(t_L)_B$, normalized by the SEF background and every value is a kind of signal-to-noise ratio, indeed (Figs. 2f, 3b, 3c):

$$G(t_L) = [E(t_L) - E(t_L)_B]/E(t_L)_B. \quad (5)$$

In the PGF, structures like "humps" are manifested more clearly and the time resolution of the method is directly revealed.

2.2 CLEAN and Lomb-Scargle methods

Two alternative methods, namely CLEAN and Lomb-Scargle, were applied to search for periodicity in the RLC of the three data sets defined in Section 1.

The CLEAN method is an algorithm proposed by Roberts, Lehar & Dreher (1987). It iteratively identifies and removes the most prominent frequency component in the data. The subtraction is performed in a way that minimizes the residual error between the observed data and the reconstructed data with the selected component removed. After subtracting a periodic component, the algorithm updates the power spectrum of the remaining data. The frequency corresponding to the next strongest periodic signal is then selected for the next iteration. This process continues until a stopping criterion is met, such as a predefined number of iterations or a certain level of residual error. The frequencies at which the algorithm successfully removes components indicate the presence of periodic signals in the time series data.

The Lomb-Scargle method (Lomb 1976; Scargle 1982) is based on Fourier analysis. Unlike traditional Fourier analysis, which relies on evenly spaced time-series, the Lomb-Scargle periodogram employs a least-squares fitting procedure that accommodates irregularly sampled data, ensuring accurate frequency estimation. It provides a robust approach for identifying periodic signals in non-uniformly sampled data.

3 Results

We demonstrate how the SEF and PGF methods work by using the "earlier" data set from the historical LC of η Car. The results are shown in Fig. 2.

Both methods require uniformly spaced data in the LC. Resampling of the LC is performed by linear interpolation with a step of $\delta t = 0.1$ yr. Although this procedure artificially increases the number of data points from 301 to 589, this interpolation does not alter the data samples so significantly that the rebinning would introduce any new spurious period. To calculate Δm (see Eq. 1), the resampled LC was smoothed to $m_S(t)$ by moving average with a suitable WS. The proper value of the WS is set by adjusting it until it produces the most prominent peak in the PGF function. We found that WS of 4.9 yr (49 dp) ensures the maximal height of the main QP hump at 5.6 yr. However, the height of the hump depends weakly on WS value. When WS is set to 4.7 yr or 5.1 yr, the height of the hump (about 0.54 SEF units) decreases only by about 1%. The effect on the height of the QP hump at 4.9 yr is the same order. Note that due to the local smoothing, the edges of the input LC with lengths WS/2 dp each are lost and the RLC is shorter. The resampled and the smoothed LCs are shown in Fig. 2a with dots and a solid line, respectively. The RLC is shown in Fig. 2b.

The next step is to check the periodicity using the constructed SEF $E(t_L)$ and PGF $G(t_L)$. The SEF is shown in three different scales: in linear-linear scale (see Fig. 2c), in log-log scale (see Fig. 2d) and in linear-linear scale with subtracted background noise, fitted with a power law function that accounts for 90% of the SEF data points (see Fig. 2e). The constructed PGF is shown in Fig. 2f. Two periods are found: the most prominent peaks at P_1=5.6 yr is already confirmed as the orbital period of the η Car system. The second by statistical significance is the peak P_2 found at 4.9 yr. In all SEF figures, vertical segments mark the main peaks and their counterparts, while in the PGF figure, the peaks and their counterparts are shown with connecting horizontal lines. The PGF is a QP spectrum similar to the result of any periodogram method. Note that the humps of $2P_1$, as well as $2P_2$ are seen. The hump of $P_1/2$ is very high, probably due to an underestimated noise.

Finally, we show that the average profiles of the significant repetitive structures (see Figs 2g–2j), corresponding to the SEF peaks at $P_1/2$ at 2.8 yr, P_1 at 5.6 yr, $2P_1$ at 11.2 yr and P_2 at 4.9 yr. Every such profile is the signal profile $\langle a_j \rangle$, rather than $\langle |a_j| \rangle$ used in Eq. 2 for the respective SEF peak.

The resampled and smoothed LCs for the two "recent" data sets are shown in Fig. 3a with dots and a solid line, respectively. For the resampled LCs, we use a step of 0.05 yr to obtain a LCs with 1186 dp, and for the smoothed LCs – WS of 131 dp (6.5 yr). Thus, the RLC for the construction of PGF contains 1056 dp. The resulted PGF for the B band is shown in Fig. 3b and for V band in Fig. 3c. Two periods are detected again: the most prominent peak P_1, close to the known orbital period, is found at 5.7 yr. The other period P_2 is found at 4.9 yr.

We also constructed 2×2 average profiles of the significant repetitive structures in the B band (see Figs 3d–3e) and in V band (see Figs 3f–3g), responsible for the PGF hump peaks P_1 at 5.7 yr and P_2 at 4.9 yr.

It is important to discuss the scale of an error in the QP. Each significant repeating structure with length L dp (and relevant QP $P = t_L = \delta t \times L$) is imprinted in the SEF and PGF humps. The reason is that structures with lengths $L-1, L-2, ..., L-i$ dp and $L+1, L+2, ..., L+i$ dp contribute to the hump peripheries. The width of the hump is proportional to the structure length L. In other words, the choice of the resampling (binning) step affects how many neighboring bins i would be involved in the hump's shape. Therefore, the relative QP resolution, the Half Width at the Half of the Maximum (HWHM) of the hump, P_{HWHM}, should be proportional to the period. For the three data sets of the historical η Car LC, the relative QP resolution is about 5% or about 0.5 yr for P_1 (Fig. 2f). However, the peaks or the middle points of the QP humps may be determined with an error of ±1 ds or ±0.1 yr. Therefore, the QP error in this analysis is 0.1 yr. We noted that after resampling the "earlier" data set with a twice larger step of 0.2 yr, the periods occur at $P_1 = 5.6$ yr and $P_2 = 4.8$ yr with error of 0.2 yr and the PGF hump resolution is about 6%.

The structures' profiles (humps) in the SEF and PGF vary, although some irregularities are probably caused by the data fluctuations (i.e., noise D). The P_1 profile (Figs. 2h, 3d, 3f) is asymmetric. In contrast, the profile of P_2 (Figs. 2i, 3e, 3g) is more or less symmetric, similarly to the profile of $P_1/2$ (Fig. 2g). Moreover, the profile of $2P_1$ (L=112) nearly reproduces the doubled shape of P_1 (Fig. 2j) but is significantly more complex. The shape of the odd

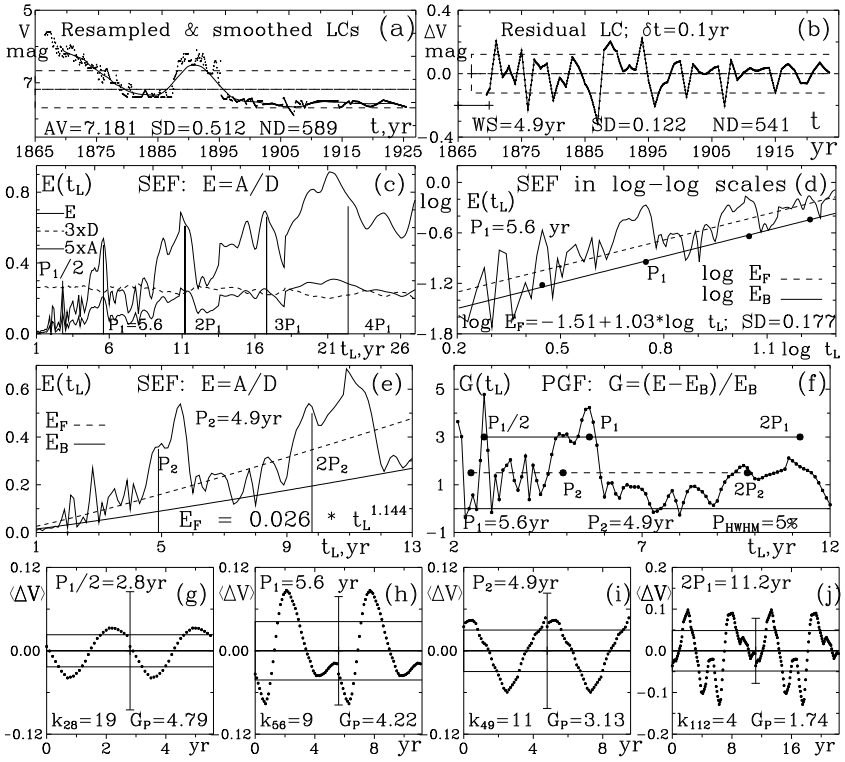

Fig. 2. Periods and the corresponding humps profiles found in the "earlier" data set of the historical LC of η Car in Fig. 1 by the means of the SEF and PGF methods (a, b, c, d, e, f). In (c), the dependencies $\mathrm{D}(t_L)$ and $\mathrm{A}(t_L)$ are scaled up 3 and 5 times, respectively, for a better view. In (e), E_F and E_B are power law fits to the SEF, shown in (d) and (e), and the SEF background that accounts for 90% of the SEF data points, respectively. In (g–j) the profiles of the prominent periods are given in terms of $\langle \Delta V \rangle = a_j$ as a function of time $j \times \delta t$, $j = 1, 2, ..., L$ for twofolded period with length 2L. The derived parameters are shown in the panels. See Section 3 for details.

and even maxima seems very different. Note that each point in that profile is averaged only k_{112}=4 times.

The results from CLEAN and Lomb-Scargle methods applied on the "earlier" and "recent" data extracted from the historical LC of η Car are shown in Figs. 4a–c. Both methods found 2 periods in the periodograms of the three data sets. In the "earlier" data set, the identified periods are $P_1 = 5.6$ yr and $P_2 = 4.9$ yr and in the "recent" data sets - $P_1 = 5.7$ yr and $P_2 = 4.9$ yr. The results of CLEAN and Lomb-Scargle application on the studied data sets are in complete agreement with the results obtained from the SEF and PGF methods.

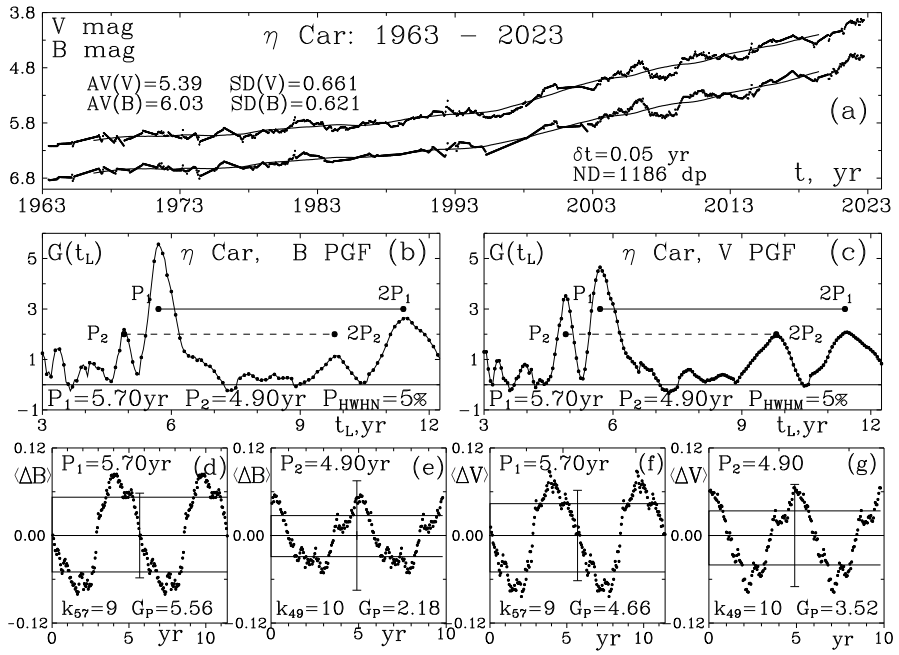

Fig. 3. Periods and the corresponding humps profiles found in the "recent" B- and V-data sets of the historical η Car LC in Fig. 1 by the means of the PGF method. In (d–g) the profiles of the prominent periods are given in terms of $\langle \Delta V \rangle$ or $\langle \Delta B \rangle = a_j$ as a function of time $j \times \delta t$, $j = 1, 2, ..., L$ for twofolded period with length 2L. Relevant parameter values derived in the analyses and used dependencies are stated in the panels. See the text in Section 3 for details.

4 Discussion

The periodicity of η Car has been discussed in various studies so far (Whitelock et al. 2004; van Genderen et al. 2006; Damineli et al. 2008; Smith & Frew 2011). The most prominent and indisputable period is the 5.5-yr orbital period associated with the binary system. Despite it, some studies suggest that η Car shows periodicity on short-terms. Variability of 85 days in X-rays is reported by Davidson, Ishibashi & Corcoran (1998) who interpreted it as a pulsation or rotation period of the primary. Another two coherent and even shorter oscillations of 23 and 59 d are discovered in η Car LC by Richardson et al. (2018). They may represent tidally excited modes of η Car's primary star during the periastron but with amplitudes smaller than two orders. We checked the "recent" V-band data that have the best coverage with a Lomb-Scargle algorithm but no significant period on that time scale is seen. Our analysis of the three data sets from the historical η Car's LC leads to the detection of another long-term period of 4.9 years, which is best manifested in the "recent" V-band data (see Fig. 3c) and less prominent in the "earlier" V-band (Figs. 2c–f) and the "recent" B-band data (see Fig. 3b). The natural explanation for these differences is that "earlier" by-eye visual photometry is less accurate and

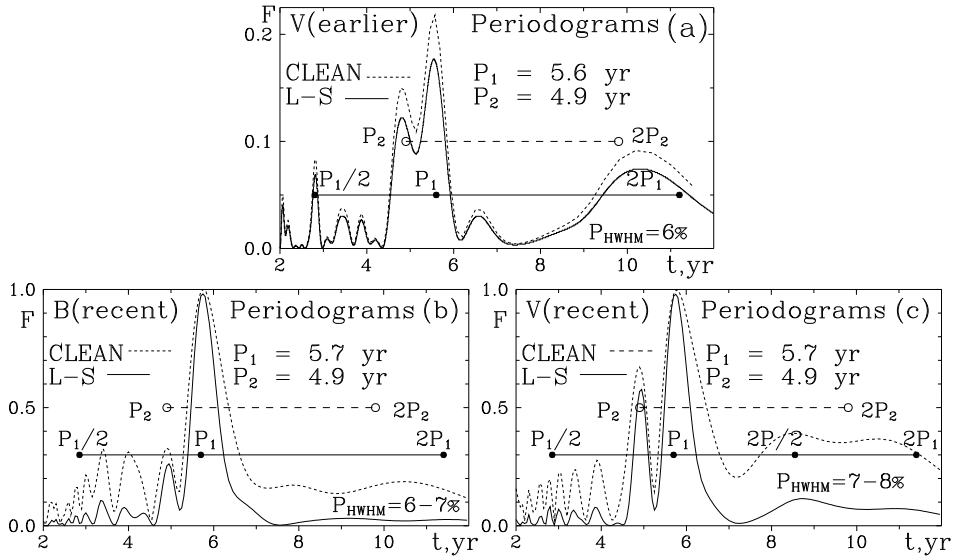

Fig. 4. Periodograms from CLEAN and Lomb-Scargle methods. **(a):** For the "earlier" V-band data set of the historical η Car LC in Fig. 1. **(b,c):** For "recent" B and V-data sets in Fig. 1

.

has lower time resolution than the "recent" V-data, while the "recent" B-band series are more sparsely sampled in comparison to the 'recent' V-band series.

The light curve of η Car does not exhibit a straightforward eclipsing pattern nor a simple hump-like variation. Examination of the near-infrared (NIR) light curves presented by Whitelock et al. (2004) and Mehner et al. (2014) reveals the presence of double "humps" both preceding and following the putative periastron passage. Notably, the temporal interval between the hump immediately following the passage and the subsequent hump prior to the next passage (approximately 5.5 years later) is approximately 5.1 years. Given that a significant portion of the NIR emissivity originates from a relatively compact region within 100 au of the primary star, the perturbed region or volume in the optical is potentially much larger, leading to an earlier manifestation of these effects on the light curve. Consequently, the observed timing between apparent humps may be shortened, which can account for the QP=4.9 yr identified in this study.

Concluding remarks

We have searched for periodicities in a compiled two centuries historical LC of the famous η Car binary system. We selected three photometric datasets for our analysis. The "earlier" data set contains V-band photometry from 1866 to 1926 and the "recent" two data sets contain B and V data from 1963-2023. We applied four periodogram methods: SEF, PGF, CLEAN and Lomb-Scargle.

SEF and the PGF based on it require uniformly spaced and smoothed data in the LCs, so the analysis was performed after such modifications.

We obtained P_1=5.6 yr based on the "earlier" LC and P_1=5.7 yr based on the "recent" LC. The uncertainty in determination of these periods is about 0.05 - 0.1 yr, which does not make the change of ΔP_1=0.1 yr significant but it is confirmed by all methods applied in our analysis. It has been suggested that close to the periastron the orbital period may increase possibly due to the enhanced ejection of mass (see Smith & Frew 2011), and though much less probable - to decrease, due to the accretion of matter (Kashi & Soker 2010). However, as η Car kept ejecting its mass by eruptions or via its very thick stellar wind, the mass of the primary keeps decreasing. Hence, the orbital period would alter gradually (yet progressively) at detectable levels within a century that is the timing between our "earlier" and "recent" LC data.

We found a second long-term period P_2=4.9±0.1 yr shorter than the 5.1 yr period of the double "humps" that the LC of η Car exhibits in the NIR before and after P=5.5 periastron passages and explain it with emissivity in the optical that originates in a larger volume.

Acknowledgments: We especially thank the anonymous referee for the valuable recommendations and suggestions that help to greatly improve the paper.
This study is financed by the European Union – NextGenerationEU, through the National Recovery and Resilience Plan of the Republic of Bulgaria, project SUMMIT BG-RRP-2.004-0008-C01. We also acknowledge the partial support of the Bulgarian National Roadmap for Research Infrastructure Project D01-326/04.12.2023 of the Ministry of Education and Science of the Republic of Bulgaria. We acknowledge with thanks the variable star observations from the AAVSO International Database contributed by observers worldwide and used in this research.

References

Damineli, A., Conti, P. S., Lopes, D. F. 1997, *New Astronomy*, 2, 2.
Damineli, A., Hillier, D. J., Corcoran, M. F., et al. 2008, *MNRAS* 384 (4), 1649.
Davidson, K., Ishibashi, K. & Corcoran, M. F 1998, *New Astronomy*, 3, 241
Feinstein, A. 1967, *The Observatory*, 87, 287.
Feinstein, A. & Marraco, H. G. 1974, *A&A*, 30, 271.
Fernández-Lajús, E., Farina, C., Torres, A. F., et al. 2009, *A&A*, 493, 1093.
Frew, D. J. 2004, *J. Astron. Data* 10, 6.
Georgiev, Ts., Boeva, S., Latev, G. et al. 2021, *Bulg.AJ*, 34, 10.
Georgiev, Ts., Boeva, S., Stoyanov, K. A., et al. 2022, *Bulg.AJ* 37, 62.
Georgiev, Ts. 2023, *Bulg.AJ* 38, 120-129 [G23]
Georgiev, Ts., Zamanov, R., Stefanov, S., 2023,*Bulg.AJ* 38, 68.
Grant D., Blundell, K., Godden, E., et al. 2023 *MNRAS*, 526, 6155.
Hirai, R., Podsiadlowski, Ph., Owocki, S. P., Schneider, F. R. N., Smith, N. 2021, *MNRAS*, 503, 4276.
Hoffleit, D. 1933, *Harvard College Observatory Bulletin*, 893, 11.
Kashi, A. & Soker, N. 2010, *ApJ*, 723, 602
Lomb N. R. 1976, *Ap&SS* 39, 447.
Mehner, A., Ishibashi, K. et al. 2014, *A&A*, 564, A14
Morse, J. A. & Smith, N. 2024, *MNRAS*, 527, 9176.
O'Connell D. J. K; S. J. 1956, *Vistas in Astronomy*, 2, 1165.
Richardson, N. D. et al. 2018, *MNRAS*, 475, 5417.
Roberts, D. H., Lehar J. & Dreher J. W. 1987, *AJ*, 93, 968.
Scargle J. D. 1982, *ApJ* 263, 835.

Strawn, E.; Richardson, N. D.; Moffat, A. F. J. 2023, *MNRAS*, 475, 5417.
Sterken, C., de Groot, . J. H., van Genderen, A. M. 1996, *A&AS*, 116, 9.
Sterken, C., Freyhammer, L., Arentoft, T., van Genderen A. M. 1999, *A&A*, 346, L33.
Shull, J. M., Darling, J., Danforth, C. W. 2021 *ApJ*, 914, 18.
Smith, N. 2006, *ApJ*, 644, 1151.
Smith, N. & Frew, D. J. 2011, *MNRAS*, 415, 2009.
Smith, N., Rest, A., Andrews, J. E. et al. 2018, *MNRAS*, 480, 1457.
van Genderen, A. M., de Groot, M. J. H & Thé, P. S. 1994, *A&A* 283, 89.
van Genderen, A. M, Sterken, C, Allen, W. H., Walker, W. S. G. 2006, *The Journal of Astronomical Data*, 12, 3.
Whitelock, P. A., Feast, M. W., Marang, F., Breedt, E. 2004, *MNRAS*, 352, 447.
NIST: Engineering Statistics Handbook, Section 1.3.5.11.
https://www.itl.nist.gov/div898/handbook/eda/sectio